

# Blindly Assess Quality of In-the-Wild Videos via Quality-aware Pre-training and Motion Perception

Bowen Li, Weixia Zhang, *Member, IEEE*, Meng Tian, *Member, IEEE*, Guangtao Zhai, *Senior Member, IEEE*, and Xianpei Wang

**Abstract**—Perceptual quality assessment of the videos acquired in the wilds is of vital importance for quality assurance of video services. The inaccessibility of reference videos with pristine quality and the complexity of authentic distortions pose great challenges for this kind of blind video quality assessment (BVQA) task. Although model-based transfer learning is an effective and efficient paradigm for the BVQA task, it remains to be a challenge to explore *what* and *how* to bridge the domain shifts for better video representation. In this work, we propose to transfer knowledge from image quality assessment (IQA) databases with authentic distortions and large-scale action recognition with rich motion patterns. We rely on both groups of data to learn the feature extractor. We train the proposed model on the target VQA databases using a mixed list-wise ranking loss function. Extensive experiments on six databases demonstrate that our method performs very competitively under both individual database and mixed database training settings. We also verify the rationality of each component of the proposed method and explore a simple manner for further improvement.

**Index Terms**—Blind video quality assessment, transfer learning, list-wise ranking loss, in-the-wild videos.

## I. INTRODUCTION

THE Global Internet Phenomena declares that video streaming has already made up more than 60% of the whole Internet traffic [1]. And a report by Cisco projects shows that online videos will account for more than 82% of all consumer Internet traffic by 2022 [2]. Confronted With various video providers, consumers expect favorable quality-of-experience (QoE) [3] when they are paying for these video services. Therefore, video quality assessment (VQA) is highly desired to develop.

The subjective quality study is the most reliable methodology for the VQA task. However, conducting such testing is labor-intensive and time-consuming, resulting in poor scalability to large-scale applications. As an alternative, objective VQA aims at automatically predicting the quality of videos quality. Objective VQA includes three categories: full-reference (FR) VQA, reduced-reference (RR) VQA, and no-reference/blind (NR/B) VQA. FR(RR)-VQA methods (par-

This work was supported in part by the National Natural Science Foundation of China under Grant 61901262, 52177109, and 51707135, in part by the Key R&D Program of Hubei Province, China under Grant 2020BAB109, in part by Fundamental Research Funds for the Central Universities, China under Grant 2042019kf1014.

Bowen Li, Meng Tian, and Xianpei Wang are with the Electronic Information School, Wuhan University, Wuhan 430072, China (e-mail: bornlee@whu.edu.cn; mengtian@whu.edu.cn; xpwang@whu.edu.cn).

Weixia Zhang, and Guangtao Zhai are with the MoE Key Laboratory of Artificial Intelligence, AI Institute, Shanghai Jiao Tong University, Shanghai 200240, China (e-mail: zwx8981@sjtu.edu.cn; zhaiguangtao@sjtu.edu.cn).

tially) rely on non-distorted videos for making quality predictions, thus are not applicable for applications where the pristine videos are inaccessible or even not existing. In this regard, increasing attention has been paid to BVQA over the past years.

Early BVQA methods were mainly developed for specific distortion types such as transmission and compression [4]–[6]. Although a plethora of general-purpose BVQA models was developed subsequently, they were still designed for handling synthetic distortions using hand-crafted features [7]–[9]. These methods usually struggle for VQA in the wild [10], where the distortions are naturally introduced during the video acquisition. Such authentic distortions may originate from multiple factors, including amateurish photographing, low-end camera devices, poor shooting environments, inappropriate post-processing, etc.

Due to the remarkable representation learning capability, deep neural networks (DNNs) have presented their promises in various vision applications over the past years. However, direct applications of the powerful DNNs for the VQA usually suffer from two main challenges: 1), prohibitively high computational complexity and memory consumption for processing the whole videos (usually with high spatial resolutions); 2), insufficient corpus with human-annotated quality labels for training effective DNNs from scratch. To mitigate the above issues, previous methods usually follow a paradigm to employ pre-trained DNNs on large-scale image databases [11] to extract frame-level features [10], [12], [13]. The philosophy behind this paradigm is straightforward because videos are composed of sequences of images. Despite being empirically effective and efficient for VQA in the wild, this paradigm inevitably confronts the problem of distributional shifts [14] between the source domains (*e.g.*, image classification) and the target domain (VQA), resulting in sub-optimal feature representation. In addition to the frame-level spatial features, motion information also plays an important role in human perception of videos [15]. However, the frame-level feature extraction paradigm inherently hinders the exploitation of spatio-temporal information for estimating the quality of videos.

In this work, we aim for dealing with the aforementioned limitations through model-based transfer learning strategies. Specifically, instead of leveraging pre-trained DNNs on object recognition [11] for feature extraction, we propose to use human-annotated IQA databases to learn quality-aware frame-level feature representation. In addition, we employ a pre-trained 3D network [16] to capture the motion information. Two groups of features are delicately aggregated, resulting in a

complementary and effective spatio-temporal video representation. Moreover, we employ a mixed list-wise ranking loss function to train the entire BVQA model, which introduces additional performance gain. We summarize our contributions as follows:

- We propose an effective and efficient method to learn a frame-level feature extractor for the VQA in the wild. We conduct a quality-aware pre-training on multiple IQA databases for transferring perceptually meaningful knowledge.
- We transfer the knowledge from an action recognition domain to perceive the motion distortion of videos. We empirically validate that the motion information is complementary to spatial features.
- We introduce a mixed list-wise ranking loss function for training the entire model, through which we obtain further performance improvement.
- Through extensive experiments, we verify that the proposed BVQA metric achieves the state-of-the-art (SOTA) results on six in-the-wild VQA databases.

## II. RELATED WORK

An intuitive solution to the BVQA task is applying BIQA metrics on videos frame by frame, followed by a scores pooling stage. In addition, motion information has also been empirically proven to play an important role in the perceived quality of videos [15]–[17]. Therefore, incorporating both spatial and motion information has become a promising paradigm for the BVQA. We briefly review related BVQA methods following this line.

### A. Classical BVQA

A plethora of classical BVQA models relies on natural scene statistics (NSS), with an underlying assumption that the quality can be measured by the disturbance of NSS [18]. NSS-based methods are derived from transform domains [19], [20], spatial domains [7], [21], or hybrid domains [22], [23]. Based on the 2D discrete-time transform (DCT) features of video frame-difference statistics, Saad *et al.* [8] further introduced motion information to enhance the representation capacity. Li *et al.* [24] captured the spatial and temporal regularities simultaneously using the 3D-DCT coefficients. Mittal *et al.* [9] designed a completely blind VQA metric by modeling the statistical naturalness of the videos by excavating the inter-subband correlations. Dendi *et al.* [25] raised an asymmetric generalized Gaussian distribution (AGGD) to model the spatio-temporal statistics using 3D mean subtract contrast normalized coefficients and bandpass filter coefficients. Another line of work is the codebook-based methodology. Motivated by CORNIA [26], Xu *et al.* [27] proposed to learn the frame-level features via an unsupervised learning method and then use the support vector regression (SVR) to map features to frame-level quality scores. The global video quality score is obtained using a temporal pooling.

### B. DNN-based BVQA

In recent years, DNNs are inclined to dominate the BVQA field. Li *et al.* [28] extracted natural scene statistics using 3D shearlet transform and then make them more discriminative using a DNN. A logistic regression function was used for training. Following an end-to-end DNN-based framework MEON [29], Liu *et al.* [30] devised a BVQA model that jointly optimizes the feature extractor, the codec classifier, and the quality predictor with a two-step training strategy. Zhang *et al.* [31] pretrained a DNN using the 3D-DCT coefficients with proxy labels. They then utilized a frequency histogram function to map the block-wise scores collected from the previous network to the perceptual quality. You *et al.* [32] designed a BVQA model with a 3D-CNN as the feature extractor and a Long-Short Term Memory (LSTM) for the overall quality prediction. Li *et al.* proposed a VSFA [10] for quality assessment of in-the-wild videos, where two crucial effects of HVS, *i.e.*, content-dependency and temporal-memory effects, are incorporated to account for quality-aware features. Based on VSFA, they then proposed a mixed databases training strategy towards a universal BVQA model (MDTVSFA) [12]. To advance progress on the prediction capabilities of real-world, in-the-wild UGC video quality, Ying *et al.* [33] created a local-to-global region-based BVQA architecture using a DNN that computes both 2D and 3D video features.

## III. PROPOSED METHOD

In this section, we first describe the quality-aware pre-training strategy for learning the frame-level feature extractor. We then incorporate motion information to form a spatio-temporal representation. Special care is taken to fuse the features in a reasonable way. Finally, we introduce a mixed list-wise ranking loss function to optimize the overall model. The framework of our model is presented in Fig. 1.

### A. Quality-aware Pre-training

The pre-training followed by fine-tuning strategy is a widely-used transfer learning paradigm due to its favorable flexibility that poses no constraint on the label spaces of the source and target domains [34], for which we have a formulation [35]:

$$f_s^* = \underset{f_s \in \mathcal{H}}{\operatorname{argmin}} \frac{1}{N_s} \sum_{i=1}^{N_s} \ell_s(f_s(x_{s,i}, q_{s,i})) + \alpha R(D_s, f_s), \quad (1)$$

where  $(x_{s,i}, q_{s,i})$  is the  $i$ -th tuple of the sample and label of the source domain,  $N_s$  is the number of samples in the source domain,  $R(\cdot)$  is a regularization term controlled by a weight  $\alpha$ , and  $f_s$  is a function that lies in a Hilbert space  $\mathcal{H}$ , which we optimize with the loss function  $\ell_s$  using the data of source domain  $D_s$ . Although being popular in VQA [10], [12], [13], the effectiveness of this paradigm is limited by distributional shifts between the source (object recognition) and target domains (VQA).

Note that videos are composed of multiple stacked images (frames), we aim for transferring the knowledge from the IQA

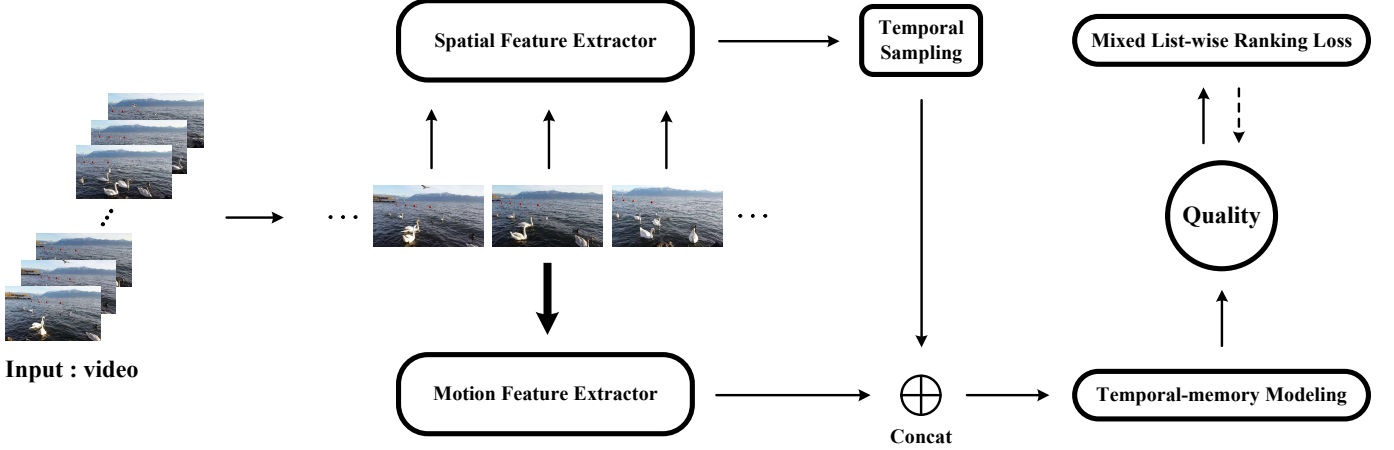


Fig. 1. The overall framework of the proposed VQA model.

databases with authentic distortions, which we assume to be source domains that better match the target domains, *i.e.*, VQA in the wild. To cover a broad range of appropriate content and authentic distortions, we consider four IQA databases with authentic distortions, *i.e.*, BID [36], LIVE Challenge [37], KonIQ-10k [38], and SPAQ [39].

It remains to specify a strategy to learn the knowledge from the IQA databases. Inspired by the database combination along with the pairwise learning-to-rank approach [40], we leverage multiple IQA datasets for pretraining the function  $f_s$ , which will serve as a frame-level feature extractor. We first formulate the loss function  $\ell_s$  to make full use of the training data. Given an image pair  $(x_s, y_s)$ , under the Thurstone's model [41], their perceptual quality  $s(x_s)$  and  $s(y_s)$  are assumed to follow a Gaussian distribution with means  $(\mu(x_s), \mu(y_s))$  and standard deviations (std)  $(\sigma(x_s), \sigma(y_s))$ . Assuming the variability of quality across images is uncorrelated, the difference  $s(x_s) - s(y_s)$  also conforms to a Gaussian distribution with mean  $\mu(x_s) - \mu(y_s)$  and std  $\sqrt{\sigma^2(x_s) + \sigma^2(y_s)}$ . Through a model parameterized by a vector  $\mathbf{w}$ , the estimated quality difference follows another Gaussian distribution with mean  $\mu_{\mathbf{w}}(x_s) - \mu_{\mathbf{w}}(y_s)$  and std  $\sqrt{\sigma_{\mathbf{w}}^2(x_s) + \sigma_{\mathbf{w}}^2(y_s)}$ . Note that  $\mu_{\mathbf{w}}(\cdot) = h_{\mu}(\phi(\cdot))$ ,  $\sigma_{\mathbf{w}}(\cdot) = h_{\sigma}(\phi(\cdot))$ , and  $f_s = \{\phi, h_{\mu}, h_{\sigma}\}$ , where  $h_{\mu}$  /  $h_{\sigma}$  and  $\phi$  denote the fully-connected (FC) layers for quality / std predictions and the backbone network, respectively. Then, the probability (Pr) that  $x_s$  is of higher perceptual quality than  $y_s$  according to the ground truths and the predicted scores can be represented respectively with:

$$\begin{aligned} p(x_s, y_s) &= \Pr(s(x_s) \geq s(y_s)) \\ &= \Phi\left(\frac{\mu(x_s) - \mu(y_s)}{\sqrt{\sigma^2(x_s) + \sigma^2(y_s)}}\right) \end{aligned} \quad (2)$$

$$\begin{aligned} p_{\mathbf{w}}(x_s, y_s) &= \Pr(s_{\mathbf{w}}(x_s) \geq s_{\mathbf{w}}(y_s)) \\ &= \Phi\left(\frac{\mu_{\mathbf{w}}(x_s) - \mu_{\mathbf{w}}(y_s)}{\sqrt{\sigma_{\mathbf{w}}^2(x_s) + \sigma_{\mathbf{w}}^2(y_s)}}\right) \end{aligned} \quad (3)$$

where  $\Phi(\cdot)$  denotes the Gaussian cumulative distribution function.

To avoid scaling ambiguity and supply  $\sigma_{\mathbf{w}}(x_s)$  with a direct supervision, we enforce a regularizer of  $\sigma_{\mathbf{w}}(x_s)$  for uncertainty learning. For an image pair  $(x_s, y_s)$ , a binary label  $g$  is assigned as  $g(x_s, y_s) = \text{sign}(\sigma(x_s) - \sigma(y_s))$ . Empirically, the similarity of Gaussian distribution and the uncertainty of the regularizer can be measured by the fidelity loss [42] and the hinge loss as follows:

$$\begin{aligned} \ell_P\{(x_s, y_s), p; \mathbf{w}\} &= 1 - \sqrt{p(x_s, y_s) \cdot p_{\mathbf{w}}(x_s, y_s)} \\ &\quad - \sqrt{(1 - p(x_s, y_s)) \cdot (1 - p_{\mathbf{w}}(x_s, y_s))} \end{aligned} \quad (4)$$

$$\begin{aligned} \ell_G\{(x_s, y_s), g; \mathbf{w}\} &= \max(0, \eta - g(x_s, y_s) \cdot \\ &\quad (\sigma_{\mathbf{w}}(x_s) - \sigma_{\mathbf{w}}(y_s))) \end{aligned} \quad (5)$$

where  $\eta$  is a margin constant. Resorting to the above four IQA databases, we randomly sample more than 250,000 image pairs, resulting in a set  $\Omega = \{(x_s, y_s)_i, p_i, g_i\}_{i=1}^{N_s}$  for training. At the training stage, we utilize every batch  $\mathcal{B}$  to optimize  $\mathbf{w}$  using the overall loss:

$$\ell_s(\mathcal{B}; \mathbf{w}) = \frac{1}{|\mathcal{B}|} \sum_{\mathcal{B} \in \Omega} \ell_P\{(x_s, y_s), p; \mathbf{w}\} + \ell_G\{(x_s, y_s), g; \mathbf{w}\} \quad (6)$$

In practice, we use a variant of stochastic gradient descent (SGD) algorithm with a  $L_2$  weight decay as the regularizer  $R$  to optimize the network. Once the training is completed, we extract the frame-level features of videos using the backbone network  $\phi$ .

To verify the rationality of the proposed quality-aware pre-training strategy, we quantitatively and qualitatively demonstrate the relation between the source and target domains. Specifically, we first use the CORAL [48] as a proxy metric to measure the distance between the source and target domains. For the source domain, we combine BID, LIVE Challenge, KonIQ-10k, and SPAQ databases to obtain a total of 22,946 images and uniformly sample the same number of images from ImageNet [11] across all available object categories. As for the target domain, we acquire 3,607 videos from five in-the-wild VQA databases, *i.e.*, CVD2014 [43], KoNViD-1k [44], LIVE-Qualcomm [45], LIVE-VQC [46],



Fig. 2. Comparison with images from IQA databases and single frames of videos from VQA databases. The top row presents the images from IQA databases including BID [36], LIVE Challenge [37], KonIQ-10k [38], and SPAQ [39]. And the bottom row presents the frames of videos sampled from VQA databases covering CVD2014 [43], KoNViD-1k [44], LIVE-Qualcomm [45], LIVE-VQC [46], YouTube-UGC [47], and LSVQ [33].

and YouTube-UGC [47]. We then use the pre-trained ResNet-50 [49] on ImageNet to extract features of all samples in the source and target domains. Note that the target features of videos are the average pooling of its frame-level features. For comparison, we follow the same procedure to extract the features with the ResNet-50 learned using the proposed quality-aware pre-training method. All distance results are shown in Fig. 3. Based on the pre-trained ImageNet weights, the CORAL distances of the sampled ImageNet subset and combined IQA set to the target VQA set are 1.65e-5 and 9.85e-6, respectively. This demonstrates that the IQA is statistically closer to the target VQA domain compared with ImageNet. On the other hand, when we measure the CORAL distances based on the features learned using the quality-aware pre-training strategy, we have CORAL distances of 7.54e-5 and 1.29e-6 for ImageNet-to-VQA and IQA-to-VQA, respectively, which further verify the effectiveness of the quality-aware pre-training. To highlight this point more intuitively, we present some visual examples with representative types of realistic impairments including “Blurry”, “Grainy”, “Underexposed”, “Shaky”, “Overexposed”, and “Poor Color” in Fig. 2. Each sample is labeled with a single dominant distortion for better visualization. From Fig. 2, we can observe similar distortion visibility between images sampled from public IQA databases and single frames cropped from videos on VQA databases.

### B. Motion Perception

In addition to static spatial features, dynamic changes are deemed as the most distinctive characteristic of videos [50]. A plethora of biological researches on the primate visual structure [51]–[53] demonstrated that there are approximately 15–20% M-cells sensitive to fast temporal changes. Therefore, incorporating motion information is helpful to facilitate video quality estimation. Previous works capture motion information using various hand-crafted features such as silhouette [54] and optical flow [55]. These methods are either computationally expensive or with less representational power. We resort to a learning-based method for extracting motion features. Similar

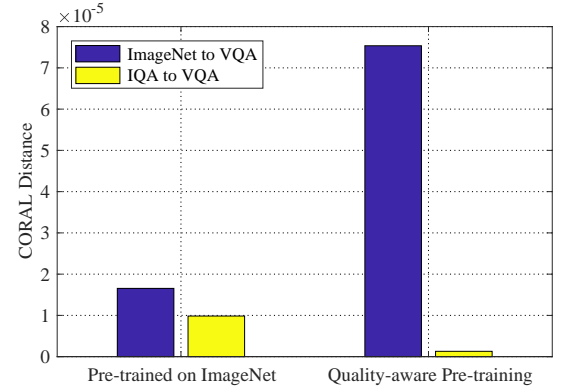


Fig. 3. The CORAL [48] distance between the source and target domains. A lower value of the CORAL distance indicates that the source and target domains are closer in the feature space.

to the model-based transfer learning philosophy stated in Section III-A, we make use of a pre-trained DNN on the action recognition to extract motion features of videos. Specifically, we resort to the fast pathway of the pre-trained SlowFast (dubbed as SlowFast<sub>F</sub>) network [16] on Kinetics-400 [56], which contains rich motion-related contents. SlowFast<sub>F</sub> can produce motion features with high temporal resolution since it maintains temporal fidelity as much as possible by prohibiting temporal downsampling before the last pooling layer. Besides, SlowFast<sub>F</sub> is formed in a lightweight manner with low channel capacity, which makes SlowFast<sub>F</sub> more computationally efficient. As a result, the extracted features are sensitive to fast motion, which is complementary to the spatial features.

As shown in Fig. 4, we exhibit continuous frames of videos sampled from Kinetics-400 and that from VQA databases and from which we observe similar distortion visibility. Specifically, all the compared videos undergo significant motion blur distortion regardless of their contents.



Fig. 4. Comparison of videos with different motion patterns. In each subgraph, the top row presents the continuous frames of videos sampled from Kinetics-400 [56], while the bottom row presents that from VQA databases including KoNViD-1k [44], LIVE-VQC [46], and LSVQ [33].

### C. Features Fusion

Let  $\{T, H \times W, C\}$  denote the temporal, spatial, and channel sizes of a raw video clip  $z = \{z_t\}_{t=1}^T$  where  $z_t$  is the  $t$ -th frame of the video.

Similar to [12], we employ ResNet-50 [49] as the backbone  $\phi$  to extract the spatial features. The network architecture is briefly summarized in “Spatial” column of Table I. To aggregate the spatial information, we leverage the activation of the last convolution of the “Spatial” pipeline. To obtain a rich spatial feature representation, we use both the global average pooling (GAP) and the global standard deviation pooling (GSP) to aggregate spatial features of a single frame as  $v_{s,t} = \text{GAP}(\phi(z_t)) \oplus \text{GSP}(\phi(z_t))$ , where  $\oplus$  denotes the concatenation operation and  $\phi(z_t)$  is with the size of  $\{T, H/32 \times W/32, 2048\}$ . As a result, we can obtain 4,096-dimensional feature vectors with a temporal length of  $T$ .

In the SlowFast<sub>F</sub> pipeline, we use the default parameters as described in [16] where the temporal stride in the slow pathway is  $\tau = 8$ , the speed and channel ratios in the fast pathway are  $\alpha = 4$  and  $\beta = 1/8$ , respectively. The network architecture is briefly summarized in the “Motion” column of Table I. Given the video clip  $z$ , SlowFast<sub>F</sub> can produce an activation with a size of  $\{T/2, H/32 \times W/32, 256\}$ . Similarly, the features are spatially pooled using GAP and GSP, resulting in a sequence of 512-dimensional frame-level features  $\{v_{m,t}\}_{t=1}^{T/2}$ .

It remains to fuse the spatial and motion features in a reasonable manner. To match the temporal resolution of the motion pipeline, we simply sample one out of every two frames along the temporal dimension of the spatial feature tensor, resulting in a 4,096-dimensional tensor with a length of  $T/2$ . We then concatenate the spatial and motion features along the channel dimension as  $v_t = v_{s,t} \oplus v_{m,t}$ . Finally, we have 4,608-dimensional frame-level feature vectors with a temporal length of  $T/2$ .

TABLE I  
THE ARCHITECTURES OF THE “SPATIAL” AND “MOTION”  
SUB-NETWORKS. THE KERNEL DIMENSIONS ARE DENOTED BY  
 $\{T \times (H \times W), C\}$  FOR TEMPORAL, SPATIAL, AND CHANNEL SIZES.  
STRIDES ARE DENOTED AS {TEMPORAL STRIDE, SPATIAL STRIDE<sup>2</sup>}

Layer	Spatial	Motion	Output size
Input	—	—	$T \times H \times W$
data layer	—	stride 2, 1 <sup>2</sup>	S: $T \times H \times W$ M: $\frac{T}{2} \times H \times W$
Conv	$1 \times 7^2, 64$ stride 1, 2 <sup>2</sup>	$5 \times 7^2, 8$ stride 1, 2 <sup>2</sup>	S: $T \times \frac{H}{2} \times \frac{W}{2}$ M: $\frac{T}{2} \times \frac{H}{2} \times \frac{W}{2}$
Pooling	$1 \times 3^2$ max stride 1, 2 <sup>2</sup>	$1 \times 3^2$ max stride 1, 2 <sup>2</sup>	S: $T \times \frac{H}{4} \times \frac{W}{4}$ M: $\frac{T}{2} \times \frac{H}{4} \times \frac{W}{4}$
ResB 1	$\begin{bmatrix} 1 \times 1^2, 64 \\ 1 \times 3^2, 64 \\ 1 \times 1^2, 256 \end{bmatrix} \times 3$	$\begin{bmatrix} 3 \times 1^2, 8 \\ 1 \times 3^2, 8 \\ 1 \times 1^2, 32 \end{bmatrix} \times 3$	S: $T \times \frac{H}{4} \times \frac{W}{4}$ M: $\frac{T}{2} \times \frac{H}{4} \times \frac{W}{4}$
ResB 2	$\begin{bmatrix} 1 \times 1^2, 128 \\ 1 \times 3^2, 128 \\ 1 \times 1^2, 512 \end{bmatrix} \times 4$	$\begin{bmatrix} 3 \times 1^2, 16 \\ 1 \times 3^2, 16 \\ 1 \times 1^2, 64 \end{bmatrix} \times 4$	S: $T \times \frac{H}{8} \times \frac{W}{8}$ M: $\frac{T}{2} \times \frac{H}{8} \times \frac{W}{8}$
ResB 3	$\begin{bmatrix} 1 \times 1^2, 256 \\ 1 \times 3^2, 256 \\ 1 \times 1^2, 1024 \end{bmatrix} \times 6$	$\begin{bmatrix} 3 \times 1^2, 32 \\ 1 \times 3^2, 32 \\ 1 \times 1^2, 128 \end{bmatrix} \times 6$	S: $T \times \frac{H}{16} \times \frac{W}{16}$ M: $\frac{T}{2} \times \frac{H}{16} \times \frac{W}{16}$
ResB 4	$\begin{bmatrix} 1 \times 1^2, 512 \\ 1 \times 3^2, 512 \\ 1 \times 1^2, 2048 \end{bmatrix} \times 3$	$\begin{bmatrix} 3 \times 1^2, 64 \\ 1 \times 3^2, 64 \\ 1 \times 1^2, 256 \end{bmatrix} \times 3$	S: $T \times \frac{H}{32} \times \frac{W}{32}$ M: $\frac{T}{2} \times \frac{H}{32} \times \frac{W}{32}$
Pooling	average	average	S: $T \times 1 \times 1$ M: $\frac{T}{2} \times 1 \times 1$
FC	$(2,048) \times 2$	256	S: $T \times 2$ M: #classes

### D. Temporal Modeling and Quality Prediction

The historic memory has been empirically proven effective for the VQA task [12], [32], [57]. Similar to [12], we take the temporal-memory effect into consideration.

We use a GRU [58] unit to model the temporal information. To enable efficient learning of the GRU, a dimension reduction

is performed to the frame-level feature vectors  $v_t$  using a FC layer:

$$\hat{v}_t = \mathcal{W}_v v_t + b_v. \quad (7)$$

where  $\mathcal{W}_v$  and  $b_v$  are learnable parameters of the FC layer. Given  $\{\hat{v}_t | t = 1, 2, \dots, T\}$  as the input fed into GRU, the hidden state at the  $t$ -th time step  $h_t$  depends on both the previous state  $h_{t-1}$  and the current input feature  $\hat{v}_t$  as:

$$h_t = \text{GRU}(\hat{v}_t, h_{t-1}) \quad (8)$$

We then use an FC layer to map the sequence of hidden states to the frame-level quality scores  $\{q_t\}_{t=1}^T$ .

As for temporal pooling, we adopt the HVS-inspired temporal hysteresis pooling [59] to aggregate the frame-level quality scores to an overall video quality score. Specifically, we implement it using a differentiable hysteresis-based temporal pooling model as [12]. Let  $\tau$  denotes the memory duration, a memory quality item  $m_t$  at the  $t$ -th frame is defined with the worst quality case across the previous frames as:

$$m_t = \begin{cases} q_t, & t = 1 \\ \min(q_k) & k \in \{\max(1, t - \tau), \dots, t - 1\}, \quad t > 1 \end{cases} \quad (9)$$

A current quality item  $c_t$  is calculated with the next  $\tau$  frames based on the fact that more rapid response will be paid into the drops in quality than the increase situation. This procedure can be established by a weighted quality combination using the softmin function as:

$$\begin{aligned} c_t &= \sum_k a_k q_k \\ a_k &= e^{-q_k} / \sum_i e^{-q_i} \\ i, k &\in \{t, \dots, \min(t + \tau, T)\} \end{aligned} \quad (10)$$

Then the hysteresis effect is expressed by a linear combination of the memory and the current quality items as:

$$q'_t = \beta m_t + (1 - \beta) c_t \quad (11)$$

where  $\beta$  is a contribution factor of different components. Finally, the entire video quality score is computed as the global average of the time-varying predicted scores:

$$Q_p = \frac{1}{T} \sum_{t=1}^T q'_t \quad (12)$$

#### E. Loss Function

An objective video quality model is expected to make quality predictions of videos consistent with subjective ratings. To this end, we employ two loss functions to encourage prediction precision and monotonicity, respectively. Following [12], [30], we adopt the Pearson Linear Correlation Coefficient (PLCC) loss to optimize our model towards higher prediction precision. As the practice in [12], we use a combination of Linear, Sigmoid, and Linear layers to model a 4-parameter logistic function [60], which is formulated as:

$$Q_m = \gamma_3 \text{Sigmoid}(\gamma_1 Q_p + \gamma_2) + \gamma_4 \quad (13)$$

where  $\{\gamma_i | i \in \{1, \dots, 4\}\}$  are the learnable fitting parameters and  $Q_m$  is the fitted quality score. Given  $N$  training samples

from a specific database, the differentiable PLCC loss then can be formulated as:

$$\begin{aligned} \ell_{\text{PLCC}} &= (1 - \text{PLCC})/2 \\ \text{PLCC} &= \frac{\sum_i (Q_m^i - \bar{Q}_m)(Q^i - \bar{Q})}{\sqrt{\sum_i (Q_m^i - \bar{Q}_m)^2 \sum_i (Q^i - \bar{Q})^2}} \end{aligned} \quad (14)$$

where  $\bar{Q}_m$  and  $\bar{Q}$  denote the mean values of the fitted predictions  $\{Q_m^i\}_{i=1}^N$  and subjective quality opinions  $\{Q^i\}_{i=1}^N$ .

To the best of our knowledge, existing BVQA methods have not explored any optimization strategy to explicitly encourage the prediction monotonicity of models. This is mainly due to the non-differentiable operations, which are frequently used for order statistics and ranking metrics. Inspired by [61], we adopt a differentiable proxy to boost the model prediction monotonicity, which is termed as a Spearman Rank-order Correlation Coefficient (SRCC) loss. In principle, the SRCC metric can be defined as the PLCC between ranks. We denote the ranks of the fitted prediction vector  $\{Q_m^i\}_{i=1}^N$  and ground-truth quality vector  $\{Q^i\}_{i=1}^N$  as  $\{Q_{mr}^i\}_{i=1}^N$  and  $\{Q_r^i\}_{i=1}^N$ , respectively, where we assume the elements of the original prediction vector are ranked in a descending order. The differentiable SRCC loss can be formulated as:

$$\begin{aligned} \ell_{\text{SRCC}} &= 1 - \text{SRCC} \\ \text{SRCC} &= \frac{\sum_i (Q_{mr}^i - \bar{Q}_{mr})(Q_r^i - \bar{Q}_r)}{\sqrt{\sum_i (Q_{mr}^i - \bar{Q}_{mr})^2 \sum_i (Q_r^i - \bar{Q}_r)^2}} \end{aligned} \quad (15)$$

where  $Q_{mr}$  and  $Q_r$  are computed from a differentiable ranking function. We refer readers to [61] for details of the process of computing "soft" ranks and the proof of its differentiability.

Finally, we can construct the overall loss:

$$\ell = \ell_{\text{PLCC}} + \lambda \ell_{\text{SRCC}} \quad (16)$$

where  $\lambda$  trades off the influence of the two elements. Note that both PLCC loss and SRCC loss are list-wise ranking loss functions, which can be used in either individual database training or mixed database training [12] settings.

## IV. EXPERIMENTS

In this section, we first describe the experimental setups, including databases, compared methods, criteria, and implementation details. We then present and analyze the results of three scenarios: individual, mixed, and cross databases. Finally, we verify the rationality of the proposed method through qualitative results, ablation study, and computational complexity analysis.

#### A. Experimental Setups

1) *Databases*: We conduct experiments on six in-the-wild VQA databases, *i.e.*, CVD2014 [43], KoNViD-1k [44], LIVE-Qualcomm [45], LIVE-VQC [46], YouTube-UGC [47], and LSVQ [33]. The main information of these databases are summarized in Table II. It is clear that they differ in content, resolution, time duration, and annotation scale, *etc*. Specially, we exclude 57 grayscale videos in YouTube-UGC for a fair comparison as [47].

TABLE II  
SUMMARY OF THE BENCHMARK IN-THE-WILD VQA DATABASES.

Database	Number of Videos	Number of Scenes	Resolution	Format	Time Duration	Max Length	Annotation Range
CVD2014 [43]	234	5	480p, 720p	RGB	10-25s	830	[-6.50, 93.38]
KoNViD-1k [44]	1,200	1,200	540p	RGB	8s	240	[1.22, 4.64]
LIVE-Qualcomm [45]	208	54	1080p	YUV	15s	526	[16.5621, 73.6428]
LIVE-VQC [46]	585	585	240p-1080p	RGB	10s	1,202	[6.2237, 94.2865]
YouTube-UGC [47]	1,380	1,380	360p-4k	YUV	20s	2,819	[1.242, 4.698]
LSVQ [33]	39,075	39,075	99p-4k	RGB	5-12s	4,096	[2.4483, 91.4194]

TABLE III

PERFORMANCE COMPARISON OF MEAN SRCC AND PLCC RESULTS ON CVD2014 [43] AND LIVE-QUALCOMM [45]. THE WEIGHTED AVERAGE RESULTS REPORT THE DATASET-SIZE (AS SHOWN IN BRACKETS) WEIGHTED RESULTS. THE BEST RESULTS ARE HIGHLIGHTED IN BOLDFACE. THE “\*” MARKED ENTRIES MEAN THAT RESULTS ARE COLLECTED FROM THEIR ORIGINAL PAPERS AND THE “—” MARKED ENTRIES DENOTE THAT THE RESULTS ARE NOT AVAILABLE.

Type	Database	CVD2014(234)		LIVE-Qualcomm(208)		Weighted average(442)	
		model	SRCC	PLCC	SRCC	PLCC	SRCC
IQA	NIQE	0.4890	0.5931	0.4628	0.4638	0.4767	0.5323
	BRISQUE	0.7086	0.7154	0.5036	0.5158	0.6121	0.6215
	FRIQUEE	0.7417	0.7682	0.6795	0.7349	0.7124	0.7525
	CORNIA	0.6140	0.6178	0.4598	0.4941	0.5414	0.5596
VQA	VIIDEO	0.0228	-0.0249	0.1267	-0.0012	0.0717	-0.0137
	V-BLIINDS	0.7458	0.7525	0.5659	0.5676	0.6611	0.6655
	TLVQM	0.83*	0.85*	78*	0.81*	0.8065	0.8312
	3D-CNN+LSTM	—	—	0.687*	0.792*	—	—
	VSFA	0.8510	0.8607	0.7083	0.7474	0.7838	0.8074
	Proposed	<b>0.8630</b>	<b>0.8764</b>	<b>0.8055</b>	<b>0.8180</b>	<b>0.8359</b>	<b>0.8489</b>

TABLE IV

PERFORMANCE COMPARISON OF MEDIAN SRCC AND PLCC RESULTS ON KONVID-1K [44], LIVE-VQC [46], AND YOUTUBE-UGC [47]. THE WEIGHTED AVERAGE RESULTS REPORT THE DATASET-SIZE (AS SHOWN IN BRACKETS) WEIGHTED RESULTS. THE BEST RESULTS ARE HIGHLIGHTED IN BOLDFACE. THE “\*” MARKED ENTRIES MEAN THAT RESULTS ARE COLLECTED FROM THEIR ORIGINAL PAPERS AND THE “—” MARKED ENTRIES DENOTE THAT THE RESULTS ARE NOT AVAILABLE.

Type	Database	KoNViD-1k(1200)		LIVE-VQC(585)		YouTube-UGC(1323)		Weighted average(3108)	
		model	SRCC	PLCC	SRCC	PLCC	SRCC	PLCC	SRCC
IQA	NIQE	0.5417	0.5530	0.5957	0.6286	0.2379	0.2776	0.4225	0.4500
	IL-NIQE	0.5264	0.5400	0.5037	0.5437	0.2918	0.3302	0.4223	0.4514
	BRISQUE	0.6567	0.6576	0.5925	0.6380	0.3820	0.3952	0.5277	0.5422
	M3	0.6578	0.6636	0.5881	0.6212	0.3678	0.3920	0.5212	0.5400
	HIGRADE	0.7206	0.7269	0.6103	0.6332	0.7376	0.7216	0.7071	0.7070
	FRIQUEE	0.7472	0.7482	0.6579	0.7000	0.7652	0.7571	0.7381	0.7429
	CORNIA	0.7169	0.7135	0.6719	0.7183	0.5972	0.6057	0.6575	0.6685
	HOSA	0.7654	0.7664	0.6873	0.7414	0.6025	0.6047	0.6814	0.6929
	VGG-19	0.7741	0.7845	0.6568	0.7160	0.7025	0.6997	0.7215	0.7355
	ResNet-50	0.8018	0.8104	0.6636	0.7205	0.7183	0.7097	0.7402	0.7506
	KonCept512	0.7349	0.7489	0.6645	0.7278	0.5872	0.5940	0.6588	0.6790
	PaQ-2-PiQ	0.6130	0.6014	0.6436	0.6683	0.2658	0.2935	0.4710	0.4829
VQA	VIIDEO	0.2988	0.3002	0.0332	0.2146	0.0580	0.1534	0.1463	0.2216
	V-BLIINDS	0.7101	0.7037	0.6939	0.7178	0.5590	0.5551	0.6427	0.6431
	TLVQM	0.7729	0.7688	0.7988	0.8025	0.6693	0.6590	0.7337	0.7284
	VIDEVAL	0.7832*	0.7803*	0.7522*	0.7514*	0.7787*	0.7733*	0.7754	0.7719
	VSFA	0.7728	0.7754	0.6978	0.7426	0.7242	0.7431	0.7380	0.7555
	RAPIQUE	0.8031*	0.8175*	0.7548*	0.7863*	0.7591*	0.7684*	0.7753	0.7907
	PVQ	0.791*	0.786*	0.827*	0.837*	—	—	—	—
	Proposed	<b>0.8362</b>	<b>0.8335</b>	<b>0.8412</b>	<b>0.8415</b>	<b>0.8312</b>	<b>0.8194</b>	<b>0.8350</b>	<b>0.8290</b>

TABLE V

PERFORMANCE COMPARISON OF MEDIAN SRCC AND PLCC RESULTS ON LSVQ [33]. THE BEST RESULTS ARE HIGHLIGHTED IN BOLDFACE. THE “\*” MARKED ENTRIES MEAN THAT RESULTS ARE COLLECTED FROM THEIR ORIGINAL PAPERS.

Type	Database	Test(7.4k)		Test-1080p(3.5k)		Weighted average(10.9k)	
		SRCC	PLCC	SRCC	PLCC	SRCC	PLCC
IQA	BRISQUE	0.579	0.576	0.497	0.531	0.5527	0.5616
VQA	TLVQM	0.772	0.774	0.589	0.616	0.7132	0.7233
	VIDEVAL	0.794	0.783	0.545	0.554	0.7140	0.7095
	VSFA	0.801	0.796	0.675	0.704	0.7605	0.7665
	PVQ(w/o)	0.814*	0.816*	0.686*	0.708*	0.7729	0.7813
	PVQ(w)	0.827*	0.828*	0.711*	0.739*	0.7898	0.7994
	Proposed	<b>0.8518</b>	<b>0.8535</b>	<b>0.7718</b>	<b>0.7878</b>	<b>0.8261</b>	<b>0.8324</b>

2) *Compared Methods*: We compare the proposed method against both BVQA and BIQA models. Note that we evolve BIQA algorithms into the baselines for video quality assessment by extracting features at each frame and then temporally average-pooling them to obtain the final features for training. The representative BIQA models are NIQE [21], IL-NIQE [62], BRISQUE [7], M3 [63], HIGRADE [64], FRIQUEE [22], CORNIA [26], HOSA [65], and pre-trained deep learning models, VGG-19 [66], ResNet-50 [49], Kon-Cept512 [38], PaQ-2-PiQ [67]. The compared BVQA methods can be roughly classified into three groups: 1), an opinion-unaware model, *i.e.*, VIIDEO [9]; 2), three shallow models including V-BLIINDS [8], TLVQM [68], and VIDEVAL [69]; and 3), five deep models involving VSFA [10], 3D-CNN+LSTM [32], MDTVSFA [12], RAPIQUE [13], and PVQ [33]. Except three training-free methods (NIQE, IL-NIQE and VIIDEO), we re-train and validate the remaining methods on the same training/validation/testing splits.

3) *Criteria*: We use two criteria to benchmark all methods. Specifically, the Spearman Rank-order Correlation Coefficient (SRCC) is used to measure the prediction monotonicity. The Pearson Linear Correlation Coefficient (PLCC) is adopted to evaluate the prediction accuracy. Before calculating PLCC, a nonlinear logistic mapping is applied as suggested in [60]. Here, we employ a four parameters mapping function. Except for LSVQ, we split each database into 60% for training, 20% for validation, and 20% for testing with no overlap of video contents. We randomly repeat this procedure ten times to prevent performance bias. Finally, the mean or median results are recorded for comparison. As for LSVQ, we follow [33] to train the model and evaluate it on two test subsets.

4) *Implementation Details*: To train the frame-level feature extractor, we minimize the loss function Eq. 6 with 250,000 image pairs. Following [40], we set the parameter  $\eta$  in Eq. 5 to 0.025. We use the pre-trained ResNet-50 on ImageNet [11] to initialize the backbone network. We run 12 epochs with a learning rate decay factor of 10 for every 3 epochs from initialization of  $10^{-4}$ . During training, the resolution of images is uniformly adjusted to  $384 \times 384 \times 3$ . For motion feature extraction, we apply the SlowFast pretrained on Kinetics-400 [56]. The instantiated sample rate (*i.e.*,  $\tau = 8$ ) on the backbone ResNet-50 as described in Section III-C is adopted. The weights of two sub-networks are frozen during the fine-tuning on the VQA datasets.

We set the hidden size of the GRU unit to 32. The duration

$\tau$  and equilibrium factor  $\alpha$  in the hysteresis-based temporal pooling are set to 12 and 0.5, respectively. During fine-tuning, all the learnable parameters are optimized using Adam [70] with a mini-batch of 32 and an initial learning rate of  $5 \times 10^{-4}$  which decays with a ratio of 0.2 for every two epochs. We fine-tune the model for 40 epochs in total. When testing, we import images with their original size. The proposed method is implemented using PyTorch, and the source code will be made publicly available at <https://github.com/zwx8981>.

### B. Performance on Individual Databases

We compare the performance on each single database in Table III, Table IV, and Table V by order of the size of databases, from which we have several interesting observations.

First, IQA methods attain meaningful performance on VQA databases, which validates their promises for the VQA task to some extent. Among them, HIGRADE and FRIQUEE achieve favorable performance by incorporating rich hand-crafted features. DNN-based methods deliver promising results, typically indicated by performance of VGG-19 and ResNet-50. These results present the advantage of the data-driven features learned from large-scale datasets over knowledge-based features. Second, by incorporating temporal information, BVQA methods generally perform competitively against adapted BIQA models, which suggests that motion information is valuable for evaluating the quality of in-the-wild videos. One exception is VIIDEO, which is calibrated to handle synthetic distortions. VSFA relies on frame-level features of pre-trained DNNs and models the temporal information using a RNN, yielding competitive performance on all databases. By incorporating local and global features in a unified framework and using a 3D network to capture temporal distortions, PVQ achieves significant performance improvement upon PaQ-2-PiQ, which provides frame-level spatial features to PVQ. Third, the proposed method learns more perceptually meaningful spatial features via a quality-aware pre-training process, transfers the motion-related knowledge from a 3D-CNN optimized on an action recognition task, and finetunes the entire model using a mixed list-wise ranking loss function. In general, our method achieves superior performance on all in-the-wild VQA databases. Typically, the proposed method outperforms VSFA on LIVE-VQC by a large margin (+14.34% SRCC). It also presents remarkable performance on larger databases (KoNViD-1k, YouTube-UGC, and LSVQ),

indicating its promising representation learning capacity on large-scale applications.

### C. Performance on Mixed Databases

1) *Database-level Mixed Test*: In a more practical experimental setting, a BVQA model is expected to perform well across different data distributions. Similar to MDTVSFA [12], we adopt a database combination strategy to train the proposed method on mixed databases. We compare with MDTVSFA by mixing the four databases including CVD2014, KoNViD-1k, LIVE-Qualcomm, and LIVE-VQC for training. The median SRCC and PLCC results are summarized in Table VI. We also apply the naive linear re-scaling (LS) [68] to integrate subjective quality scores and use L1-norm loss for regression, termed as Proposed-LS. We observe that our BVQA metric achieves consistently better performance than MDTVSFA. The mixed list-wise ranking method is superior to LS in terms of the overall performance on all databases, indicating favorable perceptual alignment across multiple databases with different scales of annotations. Taking a comparison of Table VI, Table III, and Table IV, we can observe performance improvements on CVD2014 and LIVE-Qualcomm but slight drops on KoNViD-1k and LIVE-VQC. This shows the mixed databases training strategy helps alleviating the over-fitting phenomenon on small databases while brings acceptable disturbance to the larger ones.

TABLE VI  
PERFORMANCE COMPARISON OF MEAN SRCC AND PLCC RESULTS OF DATASET-SIZE WEIGHTED VALUES ACROSS 10 SESSIONS ON CVD2014 [43], KONViD-1K [44], LIVE-QUALCOMM [45], AND LIVE-VQC [46]. THE WEIGHTED AVERAGE RESULTS REPORT THE DATASET-SIZE WEIGHTED RESULTS.

Subset		MDTVSFA	Proposed-LS	Proposed
CVD2014	SRCC	0.8341	0.8232	<b>0.8721</b>
	PLCC	0.8404	0.8224	<b>0.8849</b>
KoNViD-1k	SRCC	0.7785	0.7962	<b>0.8214</b>
	PLCC	0.7824	0.7893	<b>0.8170</b>
LIVE-Qualcomm	SRCC	0.8059	0.8097	<b>0.8431</b>
	PLCC	0.8243	0.8281	<b>0.8560</b>
LIVE-VQC	SRCC	0.7344	0.7896	<b>0.8224</b>
	PLCC	0.7687	0.7861	<b>0.8364</b>
Weighted average	SRCC	0.7753	0.7986	<b>0.8290</b>
	PLCC	0.7888	0.7956	<b>0.8329</b>

2) *Category-level Mixed Test*: We follow the three categorical evaluation methodologies in [69] to give insights into different aspects. To this end, we combine KoNViD-1k, LIVE-VQC and YouTube-UGC for training, termed as Combined<sub>U</sub>.

a) *Resolution Subsets*: According to resolution, the Combined<sub>U</sub> can be formed into three sets, *i.e.*, 427 1080p-videos, 566 720p-videos, and 448 videos with resolution no more than 480p. We list the SRCC and PLCC results in Table VII.

b) *Content Subsets*: There are plenty of researches concentrating on different content-based scenarios. It is also interesting to observe the behaviors of compared models on different contents. To this end, we conduct experiments using three typical contents, *i.e.*, 163 Screen Contents, 81 Animations, and 209 Gamings. We report the performance in Table VIII.

TABLE VII  
PERFORMANCE COMPARISON OF MEDIAN SRCC AND PLCC RESULTS ON DIFFERENT RESOLUTION SUBSETS: 1080P, 720P, AND  $\leq$ 480P FROM KONViD-1K [44], LIVE-VQC [46], AND YOUTUBE-UGC [47].

Subset model	1080p		720p		$\leq$ 480p	
	SRCC	PLCC	SRCC	PLCC	SRCC	PLCC
BRISQUE	0.4597	0.4637	0.5407	0.5585	0.3812	0.4065
M3	0.4796	0.4970	0.5098	0.5172	0.3685	0.4200
HIGRADE	0.5142	0.5543	0.5095	0.5324	0.4650	0.4642
FRIQUEE	0.5787	0.5797	0.5369	0.5652	0.5042	0.5363
CORNIA	0.5951	0.6358	0.6212	0.6551	0.5631	0.6118
HOSA	0.5924	0.6093	0.6651	0.6739	0.6514	0.6652
VGG-19	0.6440	0.6090	0.6158	0.6568	0.5845	0.6267
ResNet-50	0.6615	0.6644	0.6645	0.7076	0.6570	0.6997
V-BLIINDS	0.4449	0.4491	0.5546	0.5719	0.4484	0.4752
TLVQM	0.5638	0.6031	0.6300	0.6526	0.4318	0.4784
VIDEVAL	0.5805	0.6111	0.6296	0.6393	0.5014	0.5508
Proposed	<b>0.7283</b>	<b>0.7371</b>	<b>0.7442</b>	<b>0.7601</b>	<b>0.7399</b>	<b>0.7621</b>

TABLE VIII  
PERFORMANCE COMPARISON OF MEDIAN SRCC AND PLCC RESULTS ON DIFFERENT CONTENT SUBSETS: SCREEN CONTENT, ANIMATION, AND GAMING FROM KONViD-1K [44], LIVE-VQC [46], AND YOUTUBE-UGC [47].

Subset model	Screen Content		Animation		Gaming	
	SRCC	PLCC	SRCC	PLCC	SRCC	PLCC
BRISQUE	0.2573	0.3954	0.0747	0.3857	0.2717	0.3307
M3	0.3004	0.4244	0.2009	0.4129	0.3371	0.4185
HIGRADE	0.4971	0.5652	0.1985	0.4140	0.6228	0.6832
FRIQUEE	0.5522	0.6160	0.2377	0.4574	0.6919	0.7193
CORNIA	0.5105	0.5667	0.1936	0.4627	0.5741	0.6502
HOSA	0.4667	0.5255	0.1048	0.4489	0.6019	0.6998
VGG-19	0.5472	0.6229	0.1973	0.4700	0.5765	0.6370
ResNet-50	0.6199	0.6676	0.2781	0.4871	0.6378	0.6779
V-BLIINDS	0.3064	0.4155	0.0379	0.3917	0.5473	0.6101
TLVQM	0.3843	0.4524	0.2708	0.4598	0.5749	0.6195
VIDEVAL	0.6033	0.6610	0.3492	0.5274	0.6954	0.7323
Proposed	<b>0.7198</b>	<b>0.7592</b>	<b>0.6479</b>	<b>0.7185</b>	<b>0.7690</b>	<b>0.7547</b>

c) *Quality Subsets*: The partition based on low and high quality is a valuable way to analyze the defects and success of the proposed model, which has been adopted as an evaluation methodology in both IQA [71] and VQA [69]. We use the same threshold of 3.5536 [69] to partition Combined<sub>U</sub> into 1,558 low quality and 1,550 high quality materials, and tabulate the comparisons in Table IX.

TABLE IX  
PERFORMANCE COMPARISON OF MEDIAN SRCC AND PLCC RESULTS ON DIFFERENT QUALITY SUBSETS: LOW QUALITY AND HIGH QUALITY FROM KONViD-1K [44], LIVE-VQC [46], AND YOUTUBE-UGC [47].

Subset model	Low Quality		High Quality	
	SRCC	PLCC	SRCC	PLCC
BRISQUE	0.4312	0.4593	0.2813	0.2979
M3	0.4221	0.4715	0.2367	0.2621
HIGRADE	0.5057	0.5466	0.4714	0.4799
FRIQUEE	0.5460	0.5886	0.5061	0.5152
CORNIA	0.4931	0.5435	0.3610	0.3748
HOSA	0.5348	0.5789	0.4208	0.4323
VGG-19	0.3710	0.4181	0.3522	0.3614
ResNet-50	0.3881	0.4250	0.2791	0.3030
V-BLIINDS	0.4703	0.5060	0.3207	0.3444
TLVQM	0.4845	0.5386	0.4783	0.4860
VIDEVAL	0.5680	0.6056	0.5546	0.5657
Proposed	<b>0.6861</b>	<b>0.6975</b>	<b>0.6658</b>	<b>0.6797</b>

The results in Table VII, VIII, and IX suggest the proposed method is effective and robust across different resolutions,

contents, and quality levels. From Table VII and VIII, we can see that learning-based features are more powerful than hand-crafted features, especially the DNN-based model. However, Table IX demonstrates that pre-trained DNNs on image classification task struggles to handle the scenarios with different quality levels. This further verifies the effectiveness of the proposed quality-aware pre-training and motion perception methods.



(a) Three representative frames of Video A in YouTube-UGC



(b) Three representative frames of Video B in YouTube-UGC



(c) Three representative frames of Video C in YouTube-UGC



(d) Three representative frames of Video D in YouTube-UGC



(e) Three representative frames of Video E in YouTube-UGC



(f) Three representative frames of Video F in YouTube-UGC

Fig. 5. Successful cases sampled from the YouTube-UGC [47] test set. The MOSs of A to F are 1.462, 1.706, 2.983, 3.033, 4.399, and 4.526, respectively. The predictions of our model are 1.760, 2.527, 3.185, 3.277, 4.311, and 4.453, respectively. Both groups of scores conform to the ranking of A < B < C < D < E < F.

#### D. Cross-database Evaluation

A BVQA model is expected to generalize to unseen distorted videos. In this regard, we conduct cross-database evaluation by training BVQA models on one database and testing them on the other databases. We record the results in Table X, Table XI, and Table XII by the order of the size of databases. We observe that the proposed method generalizes well to



(a) Three representative frames of Video A in YouTube-UGC



(b) Three representative frames of Video B in YouTube-UGC



(c) Three representative frames of Video C in KoNViD-1k



(d) Three representative frames of Video D in KoNViD-1k

Fig. 6. Failure cases sampled from the YouTube-UGC [47] and KoNViD-1k [44] test sets. The MOSs of A and B are both 3.056 while the predictions are 3.464 and 3.187, respectively. The MOSs of C and D are 3.88 and 4.40 while the predictions are 4.017 and 3.938, respectively.

unseen databases. On small and medium scale databases, the improvement of average performance is over 7% (SRCC). For the largest database LSVQ, our method achieves more than a 4% (SRCC) boost. These performance gains demonstrate the favorable generalizability of the proposed method, which we believe is mainly due to the effectiveness of the proposed knowledge transferring strategy.

TABLE X  
CROSS-DATABASE COMPARISON OF SRCC RESULTS ON CVD2014 [43] AND LIVE-QUALCOMM [45]. THE “\*” MARKED ENTRIES MEAN THAT RESULTS ARE COLLECTED FROM THEIR ORIGINAL PAPERS.

Training	CVD2014	LIVE-Qualcomm
Testing	LIVE-Qualcomm	CVD2014
BRISQUE	0.4632	0.3930
V-BLIINDS	0.4170	0.5027
TLVQM	0.38*	0.36*
MDTVSFA	0.3919*	0.5879*
Proposed	<b>0.6696</b>	<b>0.6949</b>

#### E. Qualitative Results

In this section, we present several successful and failure samples in Fig. 5 and Fig. 6, respectively. As shown in Fig. 5, our method can distinguish quality levels even with small differences of MOSs. Then, we visualize several failure cases in Fig. 6. Among them, for the two comparisons of Video A against Video B and Video C against Video D, the quality rankings predicted by our model are not consistent with the corresponding MOSs. Note that both cases are of relatively

TABLE XI

CROSS-DATABASE COMPARISON OF SRCC AND PLCC RESULTS ON KONViD-1k [44], LIVE-VQC [46], AND YOUTUBE-UGC [47]. THE “\*” MARKED ENTRIES MEAN THAT RESULTS ARE COLLECTED FROM THEIR ORIGINAL PAPERS.

Training	KoNViD-1k				LIVE-VQC				YouTube-UGC			
	Testing		LIVE-VQC		YouTube-UGC		KoNViD-1k		YouTube-UGC		LIVE-VQC	
	SRCC	PLCC										
VIDEVAL	0.6273	0.6543	0.37*	0.39*	0.6253	0.6213	0.3023	0.3181	0.61*	0.62*	0.5417	0.5533
MDTVSFA	0.7175	0.7597	0.4237	0.4599	0.6949	0.7109	0.3538	0.3880	0.6486	0.6461	0.5816	0.6031
Proposed	<b>0.7799</b>	<b>0.7803</b>	<b>0.4747</b>	<b>0.4856</b>	<b>0.7382</b>	<b>0.7210</b>	<b>0.5964</b>	<b>0.5962</b>	<b>0.7825</b>	<b>0.7731</b>	<b>0.6521</b>	<b>0.6753</b>

TABLE XII

CROSS-DATABASE COMPARISON OF SRCC AND PLCC RESULTS WHEN THE MODELS ARE TRAINED ON LSVQ [33], THEN TESTED ON KONViD-1k [44] AND LIVE-VQC [46]. THE “\*” MARKED ENTRIES MEAN THAT RESULTS ARE COLLECTED FROM THEIR ORIGINAL PAPERS.

Training	LSVQ			
	KoNViD-1k		LIVE-VQC	
Testing	SRCC	PLCC	SRCC	PLCC
BRISQUE	0.646	0.647	0.524	0.536
TLVQM	0.732	0.724	0.670	0.691
VIDEVAL	0.751	0.741	0.630	0.640
VSFA	0.784	0.794	0.734	0.772
PVQ(w/o)	0.782*	0.781*	0.747*	0.776*
PVQ(w)	0.791*	0.795*	0.770*	0.807*
Proposed	<b>0.839</b>	<b>0.830</b>	<b>0.816</b>	<b>0.824</b>

high perceptual quality, and our method still make reasonable quality predictions although their relative rankings are not consistent with the MOSs.

### F. Ablation Study

To verify the rationality of each module of the proposed method, we conduct a series of ablation studies from the following three aspects.

First, we evaluate the effectiveness of the features fusion. We begin with a **baseline** which uses the pre-trained ResNet-50 on ImageNet as the feature extractor and use a GRU unit to model the temporal information. Then, we replace the baseline feature extractor with a ResNet-50 trained using the proposed quality-aware pre-training method (**S-Feature**) or the motion features of SlowFast<sub>F</sub> (**M-Feature**). Note that the proposed method relies on both spatial and motion features (**S+M-Feature**), and all variants are supervised with the mixed loss as described in Section III-E. We report the results in Table XIII, where we have several interesting observations. First, S-Feature alone is able to introduce a 4.16% improvement on the weighted average SRCC over the baseline, indicating the effectiveness of knowledge transfer due to the proposed quality-aware pre-training strategy. In contrast, M-Feature alone results in significant performance drop on all databases, which suggests that spatial features play vital role in perceiving the quality of videos. Combing S-Feature and M-Feature lead to the most promising results, demonstrating the complementarity between spatial and motion features for the VQA task. Typically, the motion features lead to a notable improvement (6.6% SRCC) on LIVE-VQC, where motion-related distortions are prevailing [12], [13]. We also replace GRU with average temporal pooling and then use

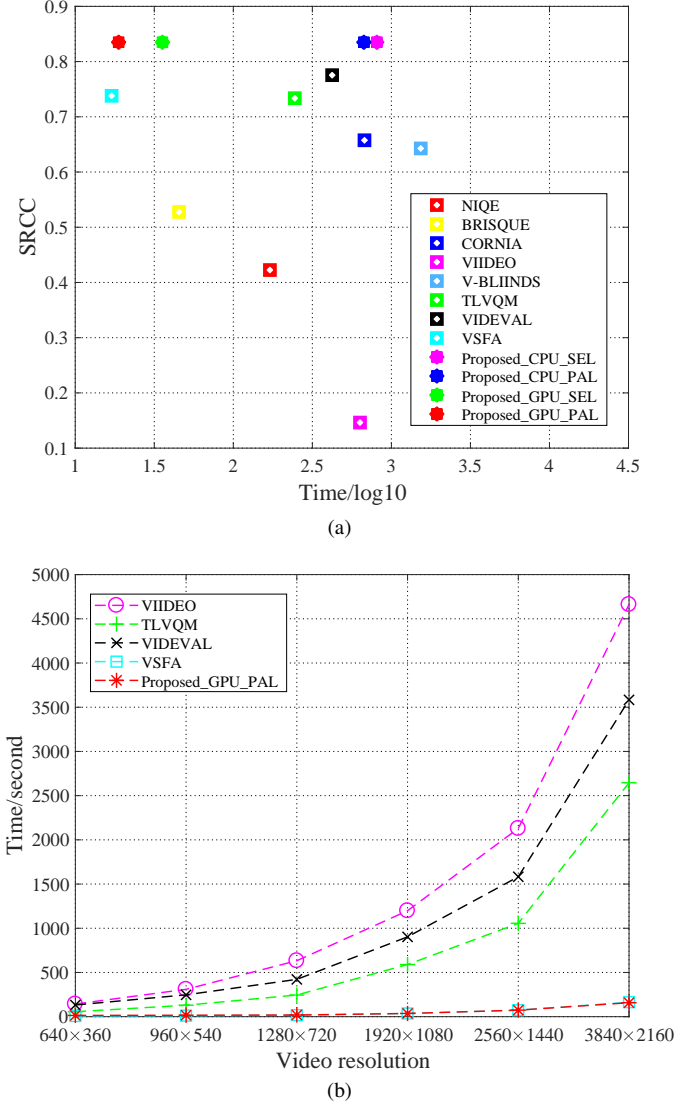


Fig. 7. (a) The weighted average SRCC results (collected from Table IV) as a function of the running time in the logarithm space. (b) The running time as a function of the video resolutions.

SVR to learn a feature-quality mapping on S-Feature (**S-Feature+SVR**). The unfavorable results suggest that modeling temporal-memory effects is of great importance.

Second, we evaluate the model trained with different loss functions, *i.e.*, linearity-induced PLCC loss, monotonicity-induced SRCC loss, and the combination of them (**Mixed**). All the variants are based on the S+M-Feature. In Table XIV, we find that both PLCC Loss and SRCC Loss alone are

TABLE XIII  
ABLATION STUDY OF DIFFERENT GROUPS OF FEATURES WHERE TAKING MEDIAN SRCC AND PLCC RESULTS FOR COMPARISON.

Database model	CVD2014		KoNViD-1k		LIVE-Qualcomm		LIVE-VQC		YouTube-UGC		Weighted average	
	SRCC	PLCC	SRCC	PLCC								
baseline	<b>0.8725</b>	<b>0.8860</b>	0.7735	0.7891	0.7533	0.7968	0.7107	0.7517	0.7879	0.7895	0.7739	0.7899
S-Feature	0.8516	0.8674	0.8272	0.8290	0.8184	0.8311	0.7752	0.7877	0.8159	0.8138	0.8155	0.8192
S-Feature+SVR	0.7583	0.7890	0.8182	0.8175	0.7400	0.7936	0.7459	0.7781	0.8174	0.8187	0.7975	0.8082
M-Feature	0.7741	0.7724	0.6649	0.6631	0.6389	0.6465	0.7245	0.7217	0.6628	0.6622	0.6796	0.6787
S+M-Feature	0.8675	0.8717	<b>0.8362</b>	<b>0.8335</b>	<b>0.8361</b>	<b>0.8389</b>	<b>0.8412</b>	<b>0.8415</b>	<b>0.8312</b>	<b>0.8194</b>	<b>0.8372</b>	<b>0.8324</b>

TABLE XIV  
ABLATION STUDY OF DIFFERENT LOSS FUNCTIONS WHERE TAKING MEDIAN SRCC AND PLCC RESULTS FOR COMPARISON.

Database model	CVD2014		KoNViD-1k		LIVE-Qualcomm		LIVE-VQC		YouTube-UGC		Weighted average	
	SRCC	PLCC	SRCC	PLCC								
PLCC Loss	0.8582	0.8563	0.8289	0.8275	0.8029	0.8226	0.8343	0.8423	0.8243	0.8115	0.8285	0.8256
SRCC Loss	0.8526	0.8632	0.8308	0.8296	0.7982	0.8120	0.8405	<b>0.8428</b>	0.8276	0.8120	0.8307	0.8264
Mixed Loss	<b>0.8675</b>	<b>0.8717</b>	<b>0.8362</b>	<b>0.8335</b>	<b>0.8361</b>	<b>0.8389</b>	<b>0.8412</b>	0.8415	<b>0.8312</b>	<b>0.8194</b>	<b>0.8372</b>	<b>0.8324</b>

TABLE XV  
ABLATION STUDY OF DIFFERENT TEMPORAL MODELING METHODS WHERE TAKING MEDIAN SRCC AND PLCC RESULTS FOR COMPARISON. THE BEST ENSEMBLE RATIO IS GIVEN IN BRACKETS.

Database model	CVD2014		KoNViD-1k		LIVE-Qualcomm		LIVE-VQC		YouTube-UGC		Weighted average	
	SRCC	PLCC	SRCC	PLCC								
GRU	0.8675	0.8717	0.8362	0.8335	0.8361	0.8389	0.8412	<b>0.8415</b>	0.8312	0.8194	0.8372	0.8324
Transformer	0.8527	0.8690	0.8382	0.8358	0.8303	0.8275	0.8355	0.8272	0.8260	0.8063	0.8337	0.8251
GRU+Transformer (Ensemble ratio)	<b>0.8703</b>	<b>0.8760</b>	<b>0.8441</b>	<b>0.8394</b>	<b>0.8529</b>	<b>0.8467</b>	<b>0.8457</b>	0.8386	<b>0.8426</b>	<b>0.8203</b>	<b>0.8460</b>	<b>0.8350</b>
	(0.67)		(0.55)		(0.65)		(0.49)		(0.41)		—	

able to yield promising results. However, there is about 0.7% additional gain brought in when combining PLCC Loss with SRCC Loss. Notably, the Mixed Loss produces relatively significant improvements on CVD2014, KoNViD-1k, and LIVE-Qualcomm.

Finally, we explore an ensemble trick to further boost the performance (see Eq. 17). As an alternative to the GRU unit, we use a Transformer [72] encoder to model the temporal information, where the number of layers, the dimension of the feed-forward network, the number of heads, and the dropout ratio are set as 2, 2048, 2, 0.2, respectively. As shown in Table XV, GRU slightly outperforms Transformer, and an ensemble of them leads to a 0.9% gain on the weighted average SRCC performance.

$$Q_e = \kappa Q_f^G + (1 - \kappa) Q_f^T \quad (17)$$

where  $Q_f^G$  and  $Q_f^T$  are the predicted scores with GRU and Transformer, respectively. The parameter  $\kappa$  is the combination factor in the ensemble procedure. And  $Q_e$  is the final ensemble quality score.

#### G. Computational Complexity

In practical applications, computational efficiency is desperately desired. We benchmark the computational complexity in this section. To make a fair comparison, all the methods are tested on the same machine, *i.e.*, a Dell Precision 7920 Tower Workstation equipped with an Intel Xeon(R) Gold 5220R CPU×2 @2.20Ghz×96, 128G RAM, and NVIDIA Quadro RTX6000 24G GPU×2. The compared models are implemented with their original released codes

on MATLAB R2020a or with Python 3.8.8, both under the Ubuntu 18.04.5 LTS operating system. We test our algorithm using CPU and GPU, respectively. Meanwhile, we adopt both serial (SEL) and parallel (PAL) modes for our proposed two groups of features. These test methods are briefly recorded as Proposed\_CPU\_SEL, Proposed\_CPU\_PAL, Proposed\_GPU\_SEL, and Proposed\_GPU\_PAL.

First, by fixing the resolution at 1280×720, we observe the relationship between the performance and the runtime, which is plotted in Fig. 7(a). Second, we evaluate the variation of runtime under different resolutions, 360p, 540p, 720p, 1080p, 1440p and 2160p, as displayed in Fig. 7(b). All the results are derived from the average of ten repeated tests that aims to remove random bias. We select a video with a resolution of 1280×720 and temporal length of 467 frames from CVD2014, and all videos with different resolutions are transformed from it. Since the feature extraction process dominates the whole computational cost, thus we compare the runtime in this procedure. Overall, we have two important conclusions. First, Fig. 7(a) shows that the proposed method (accelerated with GPU) achieves a remarkable trade-off between effectiveness and efficiency. Second, as shown in Fig. 7(b), the proposed method performs more efficiently as the resolution increases. For example, with the resolution grows from 360p to 2160p, our algorithm (Proposed\_GPU\_PAL) can achieve an increase in speed from 3 times to 16 times compared against TLVQM.

## V. CONCLUSION

We have proposed a DNN-based BVQA method for the in-the-wild scenario. We use model-based transfer learning

methods to leverage knowledge from two types of source domains, corresponding to spatial appearance and temporal motion, respectively. Specifically, we conduct a quality-aware pre-training on multiple IQA databases to learn the frame-level feature extractor, which significantly enhance the feature representation without laborious efforts on video quality annotation. Similarly, we use a pre-trained DNN on action recognition to account for the motion perception of videos, which is complementary to the spatial features. We verify the promising performance of the proposed method through extensive experiments on six in-the-wild VQA datasets. Besides, the merging of the differentiable PLCC and SRCC loss functions further boosts the performance.

In future research, we believe the efficient joint optimization of the spatio-temporal representation is a promising direction. In addition, it is also important to incorporate the viewing conditions for making quality predictions [73] of videos captured in varying environments. Another direction is developing effective continual learning methods [74], [75] for handling the BVQA where the data is streaming.

## REFERENCES

- [1] Sandvine, “The global internet phenomena report,” Sept. 2019. [Online]. Available: [https://www.sandvine.com/hubfs/Sandvine\\_Redesign\\_2019/Downloads/Internet%20Phenomena/Internet%20Phenomena%20Report%20Q32019%2020190910.pdf](https://www.sandvine.com/hubfs/Sandvine_Redesign_2019/Downloads/Internet%20Phenomena/Internet%20Phenomena%20Report%20Q32019%2020190910.pdf)
- [2] Cisco VNI, “Cisco visual networking index: Forecast and trends, 2017–2022 white paper,” *San Jose, CA 95134 USA*, 2019. [Online]. Available: [http://www.cisco.com/en/US/solutions/collateral/ns341/ns525/ns537/ns705/ns827/white\\_paper\\_c11-481360\\_ns827\\_Networking\\_Solutions\\_White\\_Paper.html](http://www.cisco.com/en/US/solutions/collateral/ns341/ns525/ns537/ns705/ns827/white_paper_c11-481360_ns827_Networking_Solutions_White_Paper.html)
- [3] Z. Duanmu, K. Zeng, K. Ma, A. Rehman, and Z. Wang, “A quality-of-experience index for streaming video,” *IEEE Journal of Selected Topics in Signal Processing*, vol. 11, no. 1, pp. 154–166, Feb. 2016.
- [4] A. Amer and E. Dubois, “Fast and reliable structure-oriented video noise estimation,” *IEEE Transactions on Circuits and Systems for Video Technology*, vol. 15, no. 1, pp. 113–118, Jan. 2005.
- [5] G. Valenzise, S. Magni, M. Tagliasacchi, and S. Tubaro, “No-reference pixel video quality monitoring of channel-induced distortion,” *IEEE Transactions on Circuits and Systems for Video Technology*, vol. 22, no. 4, pp. 605–618, Apr. 2012.
- [6] J. Søgaard, S. Forchhammer, and J. Korhonen, “No-reference video quality assessment using codec analysis,” *IEEE Transactions on Circuits and Systems for Video Technology*, vol. 25, no. 10, pp. 1637–1650, Oct. 2015.
- [7] A. Mittal, A. K. Moorthy, and A. C. Bovik, “No-reference image quality assessment in the spatial domain,” *IEEE Transactions on Image Processing*, vol. 21, no. 12, pp. 4695–4708, Dec. 2012.
- [8] M. A. Saad, A. C. Bovik, and C. Charrier, “Blind prediction of natural video quality,” *IEEE Transactions on Image Processing*, vol. 23, no. 3, pp. 1352–1365, Mar. 2014.
- [9] A. Mittal, M. A. Saad, and A. C. Bovik, “A completely blind video integrity oracle,” *IEEE Transactions on Image Processing*, vol. 25, no. 1, pp. 289–300, Jan. 2016.
- [10] D. Li, T. Jiang, and M. Jiang, “Quality assessment of in-the-wild videos,” in *ACM International Conference on Multimedia*, 2019, pp. 2351–2359.
- [11] J. Deng, W. Dong, R. Socher, L.-J. Li, K. Li, and F.-F. Li, “ImageNet: A large-scale hierarchical image database,” in *IEEE Conference on Computer Vision and Pattern Recognition*, 2009, pp. 248–255.
- [12] D. Li, T. Jiang, and M. Jiang, “Unified quality assessment of in-the-wild videos with mixed datasets training,” *International Journal of Computer Vision*, vol. 129, no. 4, pp. 1238–1257, Jan. 2021.
- [13] Z. Tu, X. Yu, Y. Wang, N. Birkbeck, B. Adsumilli, and A. C. Bovik, “RAPIQUE: Rapid and accurate video quality prediction of user generated content,” *CoRR*, vol. abs/2101.10955, 2021.
- [14] K. Zhou, Z. Liu, Y. Qiao, T. Xiang, and C. C. Loy, “Domain generalization: A survey,” *CoRR*, vol. abs/2103.02503, 2021.
- [15] K. Seshadrinathan and A. C. Bovik, “Motion tuned spatio-temporal quality assessment of natural videos,” *IEEE Transactions on Image Processing*, vol. 19, no. 2, pp. 335–350, Feb. 2010.
- [16] C. Feichtenhofer, H. Fan, J. Malik, and K. He, “SlowFast networks for video recognition,” in *International Conference on Computer Vision*, 2019, pp. 6201–6210.
- [17] Z. Tu, C.-J. Chen, L.-H. Chen, N. Birkbeck, B. Adsumilli, and A. C. Bovik, “A comparative evaluation of temporal pooling methods for blind video quality assessment,” in *IEEE International Conference on Image Processing*, 2020, pp. 141–145.
- [18] J. Yan, W. Zhang, and T. Feng, “Blind image quality assessment based on natural redundancy statistics,” in *Asian Conference on Computer Vision*, 2016, pp. 3–18.
- [19] A. K. Moorthy and A. C. Bovik, “Blind image quality assessment: From natural scene statistics to perceptual quality,” *IEEE Transactions on Image Processing*, vol. 20, no. 12, pp. 3350–3364, Dec. 2011.
- [20] M. A. Saad, A. C. Bovik, and C. Charrier, “Blind image quality assessment: A natural scene statistics approach in the DCT domain,” *IEEE Transactions on Image Processing*, vol. 21, no. 8, pp. 3339–3352, Aug. 2012.
- [21] A. Mittal, R. Soundararajan, and A. C. Bovik, “Making a “completely blind” image quality analyzer,” *IEEE Signal Processing Letters*, vol. 20, no. 3, pp. 209–212, Mar. 2013.
- [22] D. Ghadiyaram and A. C. Bovik, “Perceptual quality prediction on authentically distorted images using a bag of features approach,” *Journal of Vision*, vol. 17, no. 1, pp. 32, 1–25, Jan. 2017.
- [23] Y. Ma, W. Zhang, J. Yan, C. Fan, and W. Shi, “Blind image quality assessment in multiple bandpass and redundancy domains,” *Digital Signal Processing*, vol. 80, pp. 37–47, Sept. 2018.
- [24] X. Li, Q. Guo, and X. Lu, “Spatiotemporal statistics for video quality assessment,” *IEEE Transactions on Image Processing*, vol. 25, no. 7, pp. 3329–3342, Jul. 2016.
- [25] S. V. R. Dendi and S. S. Channappayya, “No-reference video quality assessment using natural spatiotemporal scene statistics,” *IEEE Transactions on Image Processing*, vol. 29, pp. 5612–5624, Apr. 2020.
- [26] P. Ye, J. Kumar, L. Kang, and D. Doermann, “Unsupervised feature learning framework for no-reference image quality assessment,” in *IEEE Conference on Computer Vision and Pattern Recognition*, 2012, pp. 1098–1105.
- [27] J. Xu, P. Ye, Y. Liu, and D. Doermann, “No-reference video quality assessment via feature learning,” in *IEEE International Conference on Image Processing*, 2014, pp. 491–495.
- [28] Y. Li, L.-M. Po, C.-H. Cheung, X. Xu, L. Feng, F. Yuan, and K.-W. Cheung, “No-reference video quality assessment with 3D shearlet transform and convolutional neural networks,” *IEEE Transactions on Circuits and Systems for Video Technology*, vol. 26, no. 6, pp. 1044–1057, Jun. 2016.
- [29] K. Ma, W. Liu, K. Zhang, Z. Duanmu, Z. Wang, and W. Zuo, “End-to-end blind image quality assessment using deep neural networks,” *IEEE Transactions on Image Processing*, vol. 27, no. 3, pp. 1202–1213, Mar. 2018.
- [30] W. Liu, Z. Duanmu, and Z. Wang, “End-to-end blind quality assessment of compressed videos using deep neural networks,” in *ACM Multimedia*, 2018, pp. 546–554.
- [31] Y. Zhang, X. Gao, L. He, W. Lu, and R. He, “Blind video quality assessment with weakly supervised learning and resampling strategy,” *IEEE Transactions on Circuits and Systems for Video Technology*, vol. 29, no. 8, pp. 2244–2255, Aug. 2019.
- [32] J. You and J. Korhonen, “Deep neural networks for no-reference video quality assessment,” in *IEEE International Conference on Image Processing*, 2019, pp. 2349–2353.
- [33] Z. Ying, M. Mandal, D. Ghadiyaram, and A. Bovik, “Patch-VQ: ‘Patch-ing Up’ the video quality problem,” in *IEEE Conference on Computer Vision and Pattern Recognition*, 2021, pp. 14 019–14 029.
- [34] S. J. Pan and Q. Yang, “A survey on transfer learning,” *IEEE Transactions on Knowledge and Data Engineering*, vol. 22, no. 10, pp. 1345–1359, Oct. 2010.
- [35] J. Wang and Y. Chen, *Introduction to transfer learning*, 2021. [Online]. Available: [jd92.wang/tlbook](http://jd92.wang/tlbook)
- [36] A. Ciancio, A. L. N. T. da Costa, E. A. B. da Silva, A. Said, R. Samadani, and P. Obrador, “No-reference blur assessment of digital pictures based on multifeature classifiers,” *IEEE Transactions on Image Processing*, vol. 20, no. 1, pp. 64–75, Jan. 2011.
- [37] D. Ghadiyaram and A. C. Bovik, “Massive online crowdsourced study of subjective and objective picture quality,” *IEEE Transactions on Image Processing*, vol. 25, no. 1, pp. 372–387, Jan. 2016.
- [38] V. Hosu, H. Lin, T. Sziranyi, and D. Saupe, “KonIQ-10k: An ecologically valid database for deep learning of blind image quality assessment,” *IEEE Transactions on Image Processing*, vol. 29, pp. 4041–4056, Jan. 2020.

[39] Y. Fang, H. Zhu, Y. Zeng, K. Ma, and Z. Wang, "Perceptual quality assessment of smartphone photography," in *IEEE Conference on Computer Vision and Pattern Recognition*, 2020, pp. 3674–3683.

[40] W. Zhang, K. Ma, G. Zhai, and X. Yang, "Uncertainty-aware blind image quality assessment in the laboratory and wild," *IEEE Transactions on Image Processing*, vol. 30, pp. 3474–3486, Mar. 2021.

[41] L. L. Thurstone, "A law of comparative judgment," *Psychological Review*, vol. 34, no. 4, pp. 273–286, 1927.

[42] M.-F. Tsai, T.-Y. Liu, T. Qin, H.-H. Chen, and W.-Y. Ma, "FRank: A ranking method with fidelity loss," in *International ACM SIGIR Conference on Research and Development in Information Retrieval*, 2007, pp. 383–390.

[43] M. Nuutinen, T. Virtanen, M. Vaahteranoka, T. Vuori, P. Oittinen, and J. Häkkinen, "CVD2014 – A database for evaluating no-reference video quality assessment algorithms," *IEEE Transactions on Image Processing*, vol. 25, no. 7, pp. 3073–3086, Jul. 2016.

[44] V. Hosu, F. Hahn, M. Jenadeh, H. Lin, H. Men, T. Szirányi, S. Li, and D. Saupe, "The Konstanz natural video database (KonViD-1k)," in *International Conference on Quality of Multimedia Experience*, 2017, pp. 1–6.

[45] D. Ghadiyaram, J. Pan, A. C. Bovik, A. K. Moorthy, P. Panda, and K.-C. Yang, "In-capture mobile video distortions: A study of subjective behavior and objective algorithms," *IEEE Transactions on Circuits and Systems for Video Technology*, vol. 28, no. 9, pp. 2061–2077, Sept. 2018.

[46] Z. Sinno and A. C. Bovik, "Large-scale study of perceptual video quality," *IEEE Transactions on Image Processing*, vol. 28, no. 2, pp. 612–627, Feb. 2019.

[47] Y. Wang, S. Inguva, and B. Adsumilli, "YouTube UGC dataset for video compression research," in *IEEE International Workshop on Multimedia Signal Processing*, 2019, pp. 1–5.

[48] B. Sun and K. Saenko, "Deep coral: Correlation alignment for deep domain adaptation," in *European Conference on Computer Vision*, 2016, pp. 443–450.

[49] K. He, X. Zhang, S. Ren, and J. Sun, "Deep residual learning for image recognition," in *IEEE Conference on Computer Vision and Pattern Recognition*, 2016, pp. 770–778.

[50] H. Kwon, M. Kim, S. Kwak, and M. Cho, "MotionSqueeze: Neural motion feature learning for video understanding," in *European Conference on Computer Vision*, 2020, pp. 345–362.

[51] M. Livingstone and D. Hubel, "Segregation of form, color, movement, and depth: anatomy, physiology, and perception," *Science*, vol. 240, no. 4853, pp. 740–749, May 1988.

[52] D. J. Felleman and D. C. Van Essen, "Distributed hierarchical processing in the primate cerebral cortex," *Cerebral Cortex*, vol. 1, no. 1, pp. 1–47, Jan. 1991.

[53] D. C. Van Essen and J. L. Gallant, "Neural mechanisms of form and motion processing in the primate visual system," *Neuron*, vol. 13, no. 1, pp. 1–10, Jul. 1994.

[54] M. Blank, L. Gorelick, E. Shechtman, M. Irani, and R. Basri, "Actions as space-time shapes," in *IEEE International Conference on Computer Vision*, vol. 2, 2005, pp. 1395–1402.

[55] N. Dalal, B. Triggs, and C. Schmid, "Human detection using oriented histograms of flow and appearance," in *European Conference on Computer Vision*, 2006, pp. 428–441.

[56] W. Kay, J. Carreira, K. Simonyan, B. Zhang, C. Hillier, S. Vijayanarasimhan, F. Viola, T. Green, T. Back, P. Natsev, M. Suleyman, and A. Zisserman, "The Kinetics human action video dataset," *CoRR*, vol. abs/1705.06950, 2017.

[57] W. Kim, J. Kim, S. Ahn, J. Kim, and S. Lee, "Deep video quality assessor: From spatio-temporal visual sensitivity to a convolutional neural aggregation network," in *European Conference on Computer Vision*, 2018, pp. 219–234.

[58] K. Cho, B. Van Merriënboer, C. Gulcehre, D. Bahdanau, F. Bougares, H. Schwenk, and Y. Bengio, "Learning phrase representations using RNN encoder-decoder for statistical machine translation," *CoRR*, vol. abs/1406.1078, 2014.

[59] K. Seshadrinathan and A. C. Bovik, "Temporal hysteresis model of time varying subjective video quality," in *IEEE International Conference on Acoustics, Speech and Signal Processing*, 2011, pp. 1153–1156.

[60] VQEG, "Final report from the video quality experts group on the validation of objective models of video quality assessment," 2000. [Online]. Available: <http://www.vqeg.org>

[61] M. Blondel, O. Teboul, Q. Berthet, and J. Djolonga, "Fast differentiable sorting and ranking," in *International Conference on Machine Learning*, 2020, pp. 950–959.

[62] L. Zhang, L. Zhang, and A. C. Bovik, "A feature-enriched completely blind image quality evaluator," *IEEE Transactions on Image Processing*, vol. 24, no. 8, pp. 2579–2591, Aug. 2015.

[63] W. Xue, X. Mou, L. Zhang, A. C. Bovik, and X. Feng, "Blind image quality assessment using joint statistics of gradient magnitude and Laplacian features," *IEEE Transactions on Image Processing*, vol. 23, no. 11, pp. 4850–4862, Nov. 2014.

[64] D. Kundu, D. Ghadiyaram, A. C. Bovik, and B. L. Evans, "No-reference quality assessment of tone-mapped HDR pictures," *IEEE Transactions on Image Processing*, vol. 26, no. 6, pp. 2957–2971, Jun. 2017.

[65] J. Xu, P. Ye, Q. Li, H. Du, Y. Liu, and D. Doermann, "Blind image quality assessment based on high order statistics aggregation," *IEEE Transactions on Image Processing*, vol. 25, no. 9, pp. 4444–4457, Sept. 2016.

[66] K. Simonyan and A. Zisserman, "Very deep convolutional networks for large-scale image recognition," in *International Conference on Learning Representations*, 2015, pp. 1–14.

[67] Z. Ying, H. Niu, P. Gupta, D. Mahajan, D. Ghadiyaram, and A. Bovik, "From patches to pictures (PaQ-2-PiQ): Mapping the perceptual space of picture quality," in *IEEE Conference on Computer Vision and Pattern Recognition*, 2020, pp. 3575–3585.

[68] J. Korhonen, "Two-level approach for no-reference consumer video quality assessment," *IEEE Transactions on Image Processing*, vol. 28, no. 12, pp. 5923–5938, Dec. 2019.

[69] Z. Tu, Y. Wang, N. Birkbeck, B. Adsumilli, and A. C. Bovik, "UGC-VQA: Benchmarking blind video quality assessment for user generated content," *IEEE Transactions on Image Processing*, vol. 30, pp. 4449–4464, Apr. 2021.

[70] D. P. Kingma and J. Ba, "Adam: A method for stochastic optimization," *CoRR*, vol. abs/1412.6980, 2014.

[71] X. Yu, C. G. Bampis, P. Gupta, and A. C. Bovik, "Predicting the quality of images compressed after distortion in two steps," *IEEE Transactions on Image Processing*, vol. 28, no. 12, pp. 5757–5770, Dec. 2019.

[72] A. Vaswani, N. Shazeer, N. Parmar, J. Uszkoreit, L. Jones, A. N. Gomez, Ł. Kaiser, and I. Polosukhin, "Attention is all you need," in *Annual Conference on Neural Information Processing Systems*, 2017, pp. 5998–6008.

[73] Z. Duanmu, W. Liu, Z. Wang, and Z. Wang, "Quantifying visual image quality: A bayesian view," *CoRR*, vol. abs/2102.00915, 2021.

[74] W. Zhang, D. Li, C. Ma, G. Zhai, X. Yang, and K. Ma, "Continual learning for blind image quality assessment," *CoRR*, vol. abs/2102.09717, 2021.

[75] W. Zhang, K. Ma, G. Zhai, and X. Yang, "Task-specific normalization for continual learning of blind image quality models," *CoRR*, vol. abs/2107.13429, 2021.